Journal of Controlled Release 305 (2019) 75–88

Contents lists available at ScienceDirect

Journal of Controlled Release

journal homepage: www.elsevier.com/locate/jconrel

Systemic administration of human mesenchymal stromal cells infected with polymer-coated oncolytic adenovirus induces efficient pancreatic tumor homing and infiltration

Youjin Na[a], Joung-Pyo Nam[a], JinWoo Hong[b], Eonju Oh[b], Ha Cheol Shin[c], Hyun Soo Kim[c], Sung Wan Kim[a], Chae-Ok Yun[b,*]

[a] Center for Controlled Chemical Delivery, Department of Pharmaceutics and Pharmaceutical Chemistry, University of Utah, Salt Lake City, UT 84112, USA
[b] Department of Bioengineering, College of Engineering, Hanyang University, Seoul, Republic of Korea
[c] Pharmicell Co., Ltd., Sugnam, Republic of Korea

ARTICLE INFO

Keywords:
Oncolytic adenovirus
Mesenchymal stromal cell
Gene therapy
Pancreatic cancer
Relaxin

ABSTRACT

Oncolytic adenovirus (oAd)-mediated gene therapy is a promising approach for cancer treatment because of its cancer cell-restricted replication and therapeutic gene expression. However, systemic administration of oAd is severely restricted by their immunogenic nature and poor tumor homing ability, thus oAd cannot be utilized to treat disseminated metastases. In this study, human bone marrow-derived mesenchymal stromal cell (hMSCs) was used as a viral replication-permissive carrier for oAd with an aim to improve the systemic delivery of the virus to tumor tissues. To overcome the poor delivery of oAd into hMSCs, a relaxin (RLX)-expressing oncolytic Ad (oAd/RLX), which degrades dense tumor extracellular matrix of highly desmoplastic pancreatic cancer, was complexed with biodegradable polymer (poly (ethyleneimine)-conjugated poly(CBA-DAH); PCDP), generating oAd/RLX-PCDP complex. oAd/RLX-PCDP complex enhanced the internalization of oAd into hMSC, leading to superior viral production and release from hMSCs, along with high RLX expression. Furthermore, systemic administration of oAd/RLX-PCDP-treated hMSCs elicited more potent antitumor effect compared to naked oAd/RLX or oAd/RLX-treated hMSC in pancreatic tumor model. This potent antitumor effect of systemically administered oAd/RLX-PCDP-treated hMSCs was achieved by superior viral replication in tumor tissues than any other treatment group. In conclusion, these results demonstrate that hMSCs are effective carriers for the systemic delivery of oAd to tumor sites and treatment of pancreatic cancer.

1. Introduction

Oncolytic adenovirus (oAd) has shown promising results in various clinical trials for the treatment various cancer [1]. Numerous researches have been conducted to improve the therapeutic potency of oAd by enhancing cancer-specific replication, tumor targeting, intratumoral spreading, and control of immune responses as well as development of novel transgenes [2–4]. However, oAd has several major hurdles that limit its efficacy when the virus is administered systemically. In specific, highly immunogenic capsid of Ad facilitates recognition of the virion by host immune system, leading to rapid inactivation and elimination of Ad from the blood by Ad-specific neutralizing antibodies (Abs) and other blood components [5,6]. As only systemically administrable therapeutics can target both primary and secondary tumors, recent studies have focused on the development of a carrier that can deliver oAd to tumor tissues via systemic route; one example of such approach is a hybrid vector system which is generated by complexing oAd with various nanomaterials, such as polymers, liposomes, or nanoparticles [4,7–10].

Alternatively, cell-based carrier system has been recently identified as a promising candidate for safe and efficient delivery of oAd to tumors [11]. Among cell-based carriers, mesenchymal stromal cells (MSCs) is considered as one of the best candidate for cancer therapy due to several advantageous attributes such as facile extraction and propagation, low immunogenicity, and strong tumor-tropic properties [12,13]. MSC therapy has been examined in various types of cancer including glioma, breast cancer, lung cancer, hepatoma carcinoma, and ovarian cancer [14–19]. Importantly, MSCs have outstanding abilities to protect virus

* Corresponding author at: Department of Bioengineering, College of Engineering, Hanyang University, 222 Wangsinmi-ro, Seongdong-gu, Seoul, Republic of Korea.
E-mail address: chaeok@hanyang.ac.kr (C.-O. Yun).

https://doi.org/10.1016/j.jconrel.2019.04.040
Received 22 October 2018; Received in revised form 22 April 2019; Accepted 28 April 2019
Available online 06 May 2019
0168-3659/

from immune responses and deliver virus to metastatic tumors [20–22]. However, the lack of coxsackie and adenovirus receptor (CAR) on the MSC surface lead to poor uptake of oAd by MSCs [23–25]. To this end, several groups have examined fiber-modified oAds, which do not depend on CAR for cellular internalization, to enhance viral uptake into MSCs [26,27]. In support of this, a recent clinical study examining systemically injected autologous MSCs loaded with fiber-modified oAd, ICOVIR-5, showed enhanced replication and therapeutic efficacy in metastatic neuroblastoma patients without toxicity [28,29].

In present report, we investigated oAd-polymer hybrid system to enhance cellular internalization of oAd into human MSCs (hMSC) rather than genetic modification of oAd fiber. Chemical modification of Ad surface is far less laborious than genetic modification, and this approach can also improve infection efficiency of oAd into hMSCs. Others have similarly noted that polymer coating of Ad surface can expand Ad tropism and enhance its cellular internalization into different target tissues [30–33]. A bioreducible cationic polymer, a 1.8 kDa branched poly(ethylenimine) (PEI)-conjugated poly(cystaminebis(acrylamide)-diaminohexane) (PCDP) [34] has been complexed with tumor extracellular matrix-degrading oAd expressing relaxin [35,36] via electrostatic interaction, generating oAd-PCDP complex. We investigated whether the PCDP can enhance virus internalization into hMSCs and evaluated tumor trafficking efficiency of oAd-PCDP-treated hMSC carriers, ultimately observing that oAd-PCDP-treated hMSCs elicits potent antitumor efficacy against pancreatic cancer by efficient viral replication.

2. Materials and methods

2.1. Cell culture

Human pancreatic carcinoma cell lines (AsPC-1, PANC-1, and MIA PaCa-2) were purchased from the American Type Culture Collection (ATCC, Manassas, VA). AsPC-1 cells were maintained in RPMI-1640 (Gibco BRL, Grand Island, NY) and other cells (PANC-1 and MIA PaCa-2) were cultured in high glucose Dulbecco's Modified Eagle's Media (DMEM, Gibco BRL). All media were supplemented with 10% fetal bovine serum (FBS, Gibco BRL). Cryopreserved hMSCs, which were isolated from bone marrow samples after aspiration from healthy adult male donors, were prepared as described in [37] and provided by Pharmicell Co., Ltd. (Sungnam, Korea). Cryopreserved hMSCs were thawed and used for this study. The hMSCs were maintained in low glucose DMEM with 10% FBS, and third- to eighth-passage hMSCs from were used for all experiments. All cells were grown in an incubator at 37 °C with 5% CO_2.

2.2. Preparation of PEI-conjugated poly(CBA-DAH) (PCDP)

PEI-conjugated poly(CBA-DAH) [PCDP] was synthesized as described in a previous study [34,38]. The amine group of branched PEI (Mw; 1.8 kDa; Sigma, St. Louis, MO) was reacted with the activated NHS ester of succinimidyl 3-(2-pyridyldithio) propionate) (SPDP; Sigma), and the produced PEI-SPDP was dialyzed [dialysis membrane (MWCO = 1000)] and lyophilized. Eight molar equivalent of PEI-SPDP was added to poly(CBA-DAH)-SH solution, and then the mixture was stirred for 12 h at room temperature. The final product (PCDP) was dialyzed (dialysis membrane; MWCO = 10,000) and was lyophilized. The synthesis of PCDP was estimated by measuring ^{1}H NMR (Bruker, 400 MHz, D2O). The final Mw of PCDP was calculated to be 10,600 Da using ^{1}H NMR data from [34], which was used to determine conjugation ratio of 1.8 kDa PEI to poly(CBA-DAH) by the integration of the proton spectrum peaks in the poly(CBA-DAH) (-$NCH_2CH_2CH_2CH_2CH_2CH_2NH_2$) and CH_2 of PEI.

2.3. Cytotoxicity of PCDP on hMSCs

To confirm the cytotoxicity of PCDP to hMSCs, MTT assay was performed. hMSCs were grown to 50% confluence in 96-well plates, then treated with varying polymer concentrations, up to 50 μg/mL. 25 kDa branched polyethylenimine (25 K PEI; Sigma) was used as a standard control. After 48 h, 50 μL of 3-(4,5-dimethylthiazol-2-yl)-2,5-diphenyl-tetrazolium bromide (MTT, 2 mg/mL in phosphate buffered saline (PBS); Sigma) was added and incubated for 4 h at 37 °C. Then, the supernatant was discarded, and the precipitate was dissolved with 200 μL dimethyl sulfoxide (DMSO; sigma). Plates were read on a microplate reader (Tecan Infinite M200; TecanDeutschland GmbH, Crailsheim, Germany) at 540 nm. The number of living cells in a PBS-treated cell group was analyzed for 100% cell viability.

2.4. Flow cytometry (FACS) analysis of MSC marker expression

For the FACS analysis of cell surface markers, hMSCs were suspended as a single cell with TrypLE™ Express (Gibco). After washing with PBS and FACS buffer (2% FBS in PBS), 1×10^6 cells were incubated with specific fluorescein isothiocyanate (FITC)-conjugated antibodies against CD14, CD34, CD45, or CD105, and phycoerythrin (PE)-conjugated antibody against CD73 in 200 μL PBS for 30 min. After washing twice with FACS buffer, the labeled cells were analyzed using BD FACscan (BD Biosciences, San Jose, CA). PE-IgG1 κ, FITC-IgG1 κ, and FITC-IgG2a κ were used as isotype controls. At least 10,000 events were collected and further analyzed with a FlowJo V10 software (FlowJo LLC, Ashland, OR). Antibodies recognizing CD45 or CD105 were purchased from Bio-Rad (Hercules, CA). Antibodies against CD14. CD34, or CD73 were purchased from BD Bioscience, and isotype controls (PE-IgG1 κ, FITC-IgG1 κ, and FITC-IgG2a κ) were obtained from eBioscience (San Diego, CA).

2.5. Preparation of Ads

The transduction efficiency was determined using green fluorescent protein (GFP)-expressing replication-incompetent Ad (dAd/GFP) [6]. Relaxin-expressing oncolytic Ad, oAd/RLX, was propagated and purified as described in our previous study [35]. Replication-incompetent dAd/GFP and replication-competent oAd/RLX were propagated in 293 cells and purified by CsCl gradient centrifugation. The number of viral particles (VP) were calculated from optical density measurements at 260 nm (OD_{260}), where an absorbance of 1 (OD_{260} = 1) was equivalent to 1.1×10^{12} VP/mL. Purified viruses were stored at −80 °C until use. Infections titers (plaque forming unit (PFU) per milliliter) were determined by limiting dilution assay in 293 cells [39]. The particle-to-PFU ratio for dAd/GFP and oAd/RLX was 3.2:1 and 45.4:1, respectively.

2.6. Generation of Ad-PCDP complex

To generate the Ad-PCDP complex, Ad particles (1×10^{10} VP) in PBS (pH 7.4) were mixed with varying concentrations of a cationic PCDP polymer (1×10^4, 2×10^4, 5×10^4, 1×10^5, or 2×10^5 PCDPs per Ad particle) by dropwise addition. The Ad-polymer was allowed to make a complex for 30 min at room temperature through electrostatic interaction.

2.7. Transduction efficiency of the Ad-PCDP complex in hMSCs

To determine transduction efficiency of naked dAd/GFP or dAd/GFP-PCDP complex, hMSCs were seeded at a density of 2×10^4 cells/well in a 24-well plate for 24 h before transduction. The dAd/GFP was reacted with 25 K PEI (PEI:dAd/GFP; 1×10^5) and various ratios of PCDP (PCDP:dAd/GFP; 1×10^4, 2×10^4, 5×10^4, 1×10^5, or 2×10^5 molar ratio), and hMSCs were transduced with naked dAd/GFP, dAd/

GFP-PEI, or dAd/GFP-PCDP at the multiplicity of infection (MOI) of 200. Ad-treated cells were cultured in growth medium supplemented with 5% FBS. After 72 h of incubation at 37 °C, cells were observed by fluorescence microscopy (AMG, Bothell, WA), and the GFP expression levels were quantified by measuring the absorbance at 485 nm for excitation and 535 nm for emission using a plate reader (Tecan Infinite M200; Tecan, Morrisville, NC). The results are presented as the average value of triplicate experiments.

2.8. Physicochemical characterization of the Ad-PCDP complex

The average particle sizes and surface charges of naked dAd/GFP, dAd/GFP-PEI, and dAd/GFP-PCDP complex were determined using the Zetasizer 3000HS (Malvern Instrument Inc., Worcestershire, UK) with dynamic laser scattering (DLS) at 488 nm and zeta particle analysis (90° fixed angle scattering) at 633 nm, respectively. The final size was computed as the average value of five independent determinations.

2.9. Cell viability assay

To evaluate the cell killing effect of each viral formulation, hMSCs grown to 70% confluence in 48-well plates were infected with the naked oAd, oAd/RLX-PEI, or oAd/RLX-PCDP complex at various MOIs. At 4 and 8 days post-infection, 100 μL of MTT (Sigma-Aldrich) at 2 mg/mL in PBS was added to each well and incubated at 37 °C for 4 h. The supernatant was then removed, and the precipitate was dissolved in 500 μL of DMSO (Sigma). Plates were read on a microplate reader at 540 nm. The number of living cells in a PBS-treated cell group was analyzed in an identical manner as a negative control.

2.10. Viral production assay

hMSCs were seeded in a 24-well plate at approximately 60–70% confluence. After 24 h, each cell was treated with naked oAd/RLX or oAd/RLX-PCDP complex at various MOIs for 18 h. Then, the infected cells were washed twice with PBS and incubated with DMEM (5% FBS) for 4 and 8 days. Then, both supernatant and cells were collected, and the mixture underwent three cycles of freezing and thawing. The copy number of Ad genomes was analyzed by real-time quantitative PCR (Taqman PCR detection; Applied Biosystems, Foster City, CA) as previously described [40]. Samples were amplified for 40 cycles in an ABI 7500 sequence detection system (Applied Biosystems) and analyzed in triplicate and data were processed by the SDS 19.1 software package (Applied Biosystems).

2.11. Relaxin ELISA

hMSCs (2×10^5 cells/well) in a 6-well were treated with PBS, naked oAd/RLX or oAd/RLX-PCDP complex at various MOIs. After 7 days post-infection, the supernatant was collected by centrifugation at 15,000 *g* for 10 min at 4 °C, and the level of relaxin protein was assessed by enzyme-linked immunosorbent assay (R&D Systems, Minneapolis, MN) according to the manufacturer's recommendations.

2.12. In vitro cancer cell cytotoxicity of oncolytic Ad-loaded hMSCs

hMSCs were seeded at a density of 2×10^5 cells/well in 6-well plates for 24 h and then treated with PBS, naked oAd/RLX, or oAd/RLX-PCDP complex at different MOIs for 18 h. At the same time, human pancreatic carcinoma cell lines (AsPC-1, PANC-1, and MIA PaCa-2) were plated at a density of 2×10^4 cells/well in 24-well plates for 24 h. Then, the virus-infected hMSCs were detached and 2×10^4 hMSCs were co-cultured directly with pancreatic cancer cell lines [41]. After 4 days (AsPC-1 and PANC-1) or 5 days (MIA PaCa-2), cancer cell cytotoxicity was analyzed by MTT assay and viral production was measured by real-time qPCR as described above.

2.13. Wound-healing assay

To assess wound-healing ability of oAd-PCDP-treated hMSCs and to determine the optimal MOIs of oAd-PCDP complex to hMSCs for in vivo study, a wound-healing assay was performed. In brief, hMSCs were seeded at a density of 5×10^4 cells/well in a 12-well plate for 24 h and then treated with PBS, naked oAd/RLX, oAd/RLX-PEI, or oAd/RLX-PCDP complex at different MOIs (5–20 MOI). At 18 h post treatment, a homogenous straight-line was scratched into the monolayer by a sterile plastic 100 μL micropipette tip. The debris was removed by washing the cells with serum-free medium. Migration of cells into the wound was observed by microscopic observations at different time points (0 and 30 h) and analyzed by ImageJ software (version 1.50b; U.S. National Institutes of Health, Bethesda, MD). Wound-healing activity is expressed as percentage filling of the scratched area from three independent experiments.

Wound-healing assay also performed with PEI and PCDP alone in the absence of oAd/RLX. For this experiment, final PEI and PCDP concentration was the same as those utilized to generate 5 MOI oAd/RLX-PEI and oAd/RLX-PCDP complex, respectively. hMSCs were seeded at a density of 5×10^3 cells/well in a 96-well ImageLock plate (Essen BioScience, Ann Arbor, MI). At 24 h post seeding, a homogenous straight-line was scratched into the monolayer by using 96-pin IncuCyte WoundMaker Tool (Essen BioScience Cat #4563) then the cells were treated with PEI and PCDP immediately after scratching apparatus. Migration of hMSCs into the wound was observed and analyzed by IncuCyte ZOOM™ (Essen BioScience). Wound-healing activity is expressed as percentage filling of the scratched area from three independent experiments.

2.14. Cell migration assay

To determine the tropism of hMSCs for pancreatic cancer cells, cell migration assay was performed according to previously described studies [16,42,43]. The hMSCs were treated with PBS, naked oAd, oAd-PEI, or oAd-CPDP complex (5 MOI) for 18 h, then the virus-infected hMSCs were plated in 300 μL of DMEM supplemented with 2% FBS on the upper chamber (2×10^4 cells/well). At the same time, 1×10^5 pancreatic cancer cells were plated in 800 μL DMEM supplemented with 10% FBS on the bottom chamber of a transwell plate (8 μm pore membrane; Greiner Bio-One, Monroe, NC). The virus-treated hMSCs were allowed to migrate across the membrane for 30 h at 37 °C. The cells attached to the upper chamber were removed by cotton swabs, and the migrated hMSCs in the lower chamber were fixed with methanol for 2 min. To analyze the migration ability, the cells were stained with hematoxylin and eosin (Sigma-Aldrich), and stained cells were manually counted using a light microscope in five randomly selected fields. The percent of migrated cells was calculated by normalization of negative control.

2.15. In vivo antitumor efficacy

Pancreatic cancer xenograft model was established by injecting 5×10^6 AsPC-1 cells into the subcutaneous of 6 weeks-old female nude mice ($n = 8$) (Charles River Inc., Wilmington, MA). Mice were used according to approved institutional protocols. When the tumor volume reached approximately 90 mm^3, the mice were injected intravenously with PBS, PCDP, hMSC (1×10^6 cell/200 μL in PBS), naked oAd/RLX, oAd/RLX-loaded hMSC, or oAd/RLX-PCDP-loaded hMSC (5 MOI; 5×10^8 VP/200 μL in PBS, 1×10^5 PCDP:Ad molar ratio) every 4 days (3 injections total). Tumor growth was measured every 4 days by caliper measurements and volume was calculated using the following formula: volume = $0.523\,L(W)^2$. Mouse body weight was measured every 4 days.

2.16. Histological and immunohistochemical analyses

AsPC-1 tumor tissues were harvested from mice at 72 h after 3 times intravenous injection with PBS, PCDP, hMSC (1×10^6 cell/200 μL in PBS), naked oAd/RLX, oAd/RLX-loaded hMSC, or oAd/RLX-PCDP-loaded hMSC (5 MOI; 5×10^8 VP-treated 1×10^6 cells/200 μL in PBS). Harvested tumor tissues were fixed in 10% formalin, processed for paraffin embedding, and then cut into 4 μm sections. Tumor tissue sections were stained with hematoxylin & eosin (H&E) and Masson's trichrome staining (MT), and then examined by microscopy. In addition, tumor sections were immunostained with Ad E1A-specific Ab (Abcam, Cambridge, UK) to assess viral replication. The terminal deoxynucleotidyl transferase dUTP nick end labeling (TUNEL) assay was performed to assess apoptosis according to manufacturer's instructions (Promega, Madison, WI).

2.17. Ethical statement

The study protocol was in accordance with the declaration of Helsinki. After receiving the informed consent, bone marrow was obtained from healthy donors. All the manufacturing and product testing procedures for hMSC generation were performed using good manufacturing practices (Pharmicell Co., Ltd).

All aspects of animal care and treatment were performed in a facility approved by the Association for Assessment and Accreditation of Laboratory Animal Care. All animal studies were performed according to the institutionally approved protocols of University of Utah and Hanyang University. All mice were housed for 1 week for acclimatization, and ad libitum access to food and water was provided.

2.18. Cellular uptake analysis

To compare the cellular uptake efficiency of oAd/RLX and oAd/RLX-PCDP, hMSCs were seeded on 6-well plate (1×10^5 cells/well) and grown to ~80% confluence then transduced with 5×10^9 VP of fluorescein isothiocyanate (FITC, Sigma)-labeled oAd/RLX or oAd/RLX-PCDP, along with PBS as negative control. FITC-labeled oAd/RLX was generated by reacting FITC and oAd/RLX in 500 μL 0.1 M sodium bicarbonate buffer (pH 8.5) overnight at 4 °C. FITC-labeled oAd/RLX was dialyzed (MWCO = 3500; Slide-A-Lyzer Dialysis Cassettes, Life Technologies, Grand Island, NY) to remove unconjugated FITC at 4 °C. FITC-labeled oAd/RLX-PCDP complex was generated by reacting FITC-labeled oAd/RLX with PCDP at 1×10^5 molar ratio. At 2 h post infection, hMSCs were washed with ice-cold PBS three times then fixed in 1% paraformaldehyde solution in PBS. Cellular uptake activity was quantified by measuring the FITC intensity with the BD FACScan analyzer (Beckton-Dickinson, San Jose, CA) using CellQuest software (Beckton-Dickinson).

2.19. Endosome escape analysis

hMSCs were seeded on 96-well plate at 3×10^3 cells/well overnight. hMSC was then treated with 100 MOI of naked oAd/RLX or oAd/RLX-PCDP complex, along with PBS as negative control. PCDP without oAd/RLX was administered to hMSCs at the same molar concentration as those utilized for the generation of oAd/RLX-PCDP complex. Subsequently, calcein (Sigma) was added to each well (final calcein concentration = 100 mg/mL) then the plates were incubated at 37 °C for 4 h. The samples were washed twice with ice-cold PBS and fluorescence microscope images were obtained with Incucyte (Essen Biosciences). Total number of endosome ruptured cells were counted from 4 separate images per well (total of 12 images per group) then the percentage increase in endosome ruptured cell counts by PCDP, oAd/RLX, and oAd/RLX-PCDP treatment in respect to PBS group were calculated.

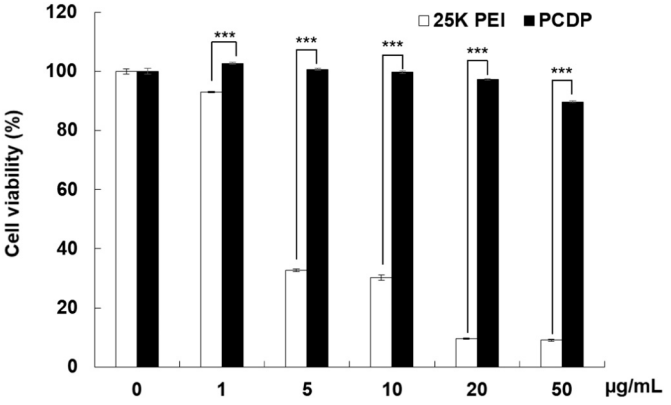

Fig. 1. Assessment of potential cytotoxic effect of PCDP polymer on hMSCs. Cells were treated with PBS, 25 K PEI, or PCDP with various concentrations. After 48 h post treatment, cytotoxicity was determined by MTT assay. Results were normalized against the PBS group. The data represent the mean ± SD of triplicates that are representative of 3 independent experiments. $^{***}P < .001$ versus 25 K PEI.

2.20. oAd and hMSC biodistribution profile analysis

Six weeks-old nude mice ($n = 3$ per group) were purchased from Charles River Korea (Seongnam, Korea). The mice were intravenously injected once with PBS, hMSC (1×10^6 cell/200 μL in PBS), naked oAd/RLX, oAd/RLX-loaded hMSC, or oAd/RLX-PCDP-loaded hMSC (5 MOI; 5×10^8 VP/200 μL in PBS, 1×10^5 PCDP:Ad molar ratio). At 24 h after the systemic administration, the lung, heart, spleen, pancreas, and liver tissues were harvested and DNA was extracted from these tissues using QIAamp DNA Blood Mini Kit (Qiagen, Hilden, Germany) according to the manufacturer's instructions. Ad biodistribution profile for oAd/RLX, oAd/RLX-loaded hMSC, or oAd/RLX-PCDP-loaded hMSC was analyzed by quantitative real-time PCR (qPCR) using Ad protein IX-specific primer set and TaqMan probe as described previously [6]. hMSC biodistribution profile for hMSC, oAd/RLX-loaded hMSC, or oAd/RLX-PCDP-loaded hMSC groups were analyzed using SYBR Green-based human Alu primer set (for the detection of hMSC in tissues) and assay protocol described elsewhere [44]. Background subtraction was performed on all experimental values by subtracting the mean value of PBS negative control group.

2.21. Transmission electron microscopy

Transmission electron microscopy (TEM) imaging of naked dAd/GFP and dAd/GFP-PCDP complexes (1×10^4 to 1×10^5 PCDP:Ad molar ratios) was carried out by incubating each sample on TEM copper grid for 5 min, performing negative staining with 2% uranyl acetate solution (Thomas Scientific, Swedesboro, NJ) then air drying at room temperature. The morphologies were subsequently characterized by TEM (JEM-2000EXll, JEPL; Nikon, Tokyo, Japan) at 200 kV. TEM-based average particle sizes of each group was obtained by measuring at least 15 particles from 8 separate TEM images.

2.22. Statistical analysis

Data were expressed as the mean ± standard deviation (SD). Statistical significance was determined by the two-tailed Student *t*-test (SPSS 13.0 software; SPSS, Chicago, IL) and ANOVA. Differences were considered statistically significant at $^{*}P < .05$, $^{**}P < .01$, or $^{***}P < .001$.

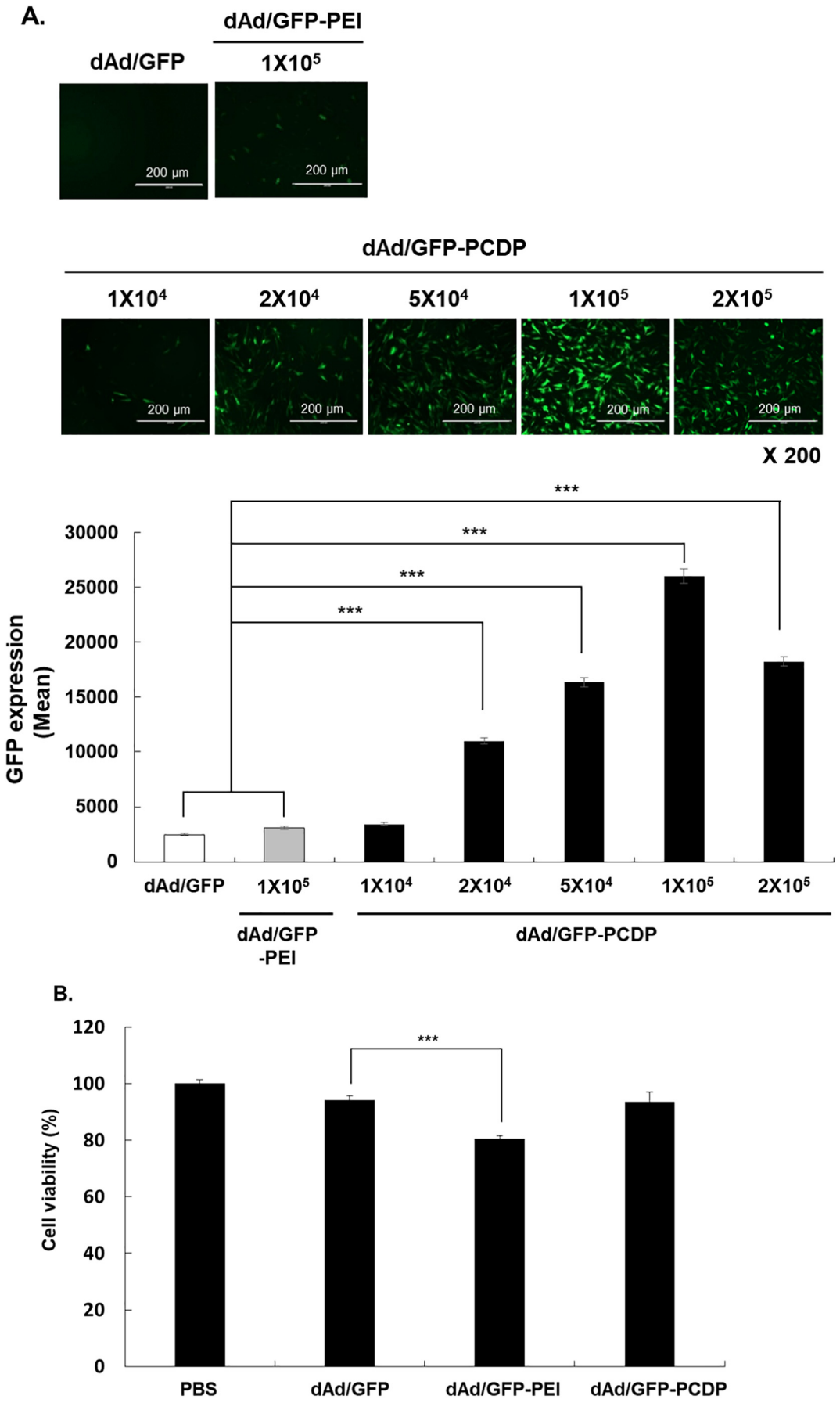

(caption on next page)

Fig. 2. Optimization of condition for the generation of dAd/GFP-PCDP complex. (A) Identification of the optimal concentration of PCDP for complexation with Ad. In vitro transduction efficiency of naked GFP-expressing Ad (dAd/GFP) or dAd/GFP complexed with different concentrations of PCDP (PCDP:Ad molar ratio of 1×10^4, 2×10^4, 5×10^4, 1×10^5, or 2×10^5). 25 K PEI was used as a control (PEI:Ad molar ratio of 1×10^5). hMSCs were transduced with 200 MOI of naked dAd/GFP, dAd/GFP-PEI, or dAd/GFP-PCDP. After 72 h post transduction, GFP expression level was analyzed by fluorescence microscopy and quantified by fluorescence reader. Original magnification, ×200. These images are representative of three independent experiments. ***$P < .001$ for dAd/GFP-PCDP versus naked dAd/GFP (B) Cytotoxicity of Ad-polymer complex. hMSCs were treated with 200 MOI of naked dAd/GFP, dAd/GFP-PEI (PEI:Ad molar ratio of 1×10^5) or dAd/GFP-PCDP (PCDP:Ad molar ratio of 1×10^5) for 72 h. Cell viability was measured by MTT assay. The data represent the mean ± SD of triplicates that are representative of 3 independent experiments. ***$P < .001$ versus naked dAd/GFP.

3. Results and discussion

3.1. Cytotoxicity analysis of PCDP

hMSCs are poorly permissive toward infection by conventional Ad due to low surface expression level of CAR [23,24,45–47]. To overcome this limitation, a cationic PCDP polymer was utilized in present report to enhance Ad internalization into hMSCs. Firstly, we assessed potential toxic effect of PCDP polymer on hMSC by incubating hMSCs with PBS, 25 kDa PEI (25 K PEI), or PCDP at concentrations ranging from 1 to 50 μg/mL for 48 h, then the cytotoxicity profile of each reagents was analyzed by MTT assay. As shown in Fig. 1**,** commercially available transfection reagent 25 K PEI induced significant toxicity at all concentrations. In marked contrast, PCDP polymer treatment led to no observable cytotoxicity up to 10 μg/mL (Fig. 1) and significantly lower toxicity than 25 K PEI at any given concentration; 89.8 ± 0.3% of hMSCs were viable at highest concentration for PCDP (50 μg/mL), whereas only 9.1 ± 0.4% was viable for 25 K PEI at the same polymer concentration ($P < .001$). Although PEI-based cationic polymers are well-known for their toxicity [48,49], PEI-based PCDP showed minimal toxicity due to the biodegradability of polymer (owing to disulfide and amide bonds in the polymer backbone).

3.2. Optimization and characterization of Ad-PCDP complex

The phenotype of hMSCs used in this study was analyzed by flow cytometry. As shown in **Fig. S1**, hMSCs were negative for both endothelial and hematopoietic cell surface markers (CD14, CD34, and CD45), and positive for bone marrow (BM) stem cell markers (CD73 and CD105), demonstrating that these cell population were pure bone marrow-derived hMSCs. To determine the optimal concentration of PCDP for complexation with Ad, transduction efficiency of GFP-expressing and non-replicating Ad (dAd/GFP) complexed with various molar ratios of PCDP (1×10^4, 2×10^4, 5×10^4, 1×10^5, or 2×10^5) was assessed in hMSCs. Branched 25 K PEI was used as a control and complexed with dAd/GFP at a molar ratio of 1×10^5, as this ratio was determined to be optimal for complexation in a previous report [50,51]. As shown in Fig. 2A, GFP expression level of the dAd/GFP-PCDP complexes (formed with Ad:PCDP molar ratio of 2×10^4 or higher) was significantly greater than that induced by naked dAd/GFP or dAd/GFP-PEI. A highest GFP expression level was observed when hMSCs were transduced with dAd/GFP-PCDP formed with molar ratio of 1×10^5 ($P < .001$). High level of transduction by Ad following complexation with PCDP was likely mediated by more efficient cellular internalization (25.8-fold increase) and endosome escaping ability (3.7-fold improvement) of the complex than naked Ad (**Fig. S4** and **S5**; $P < .001$ versus naked Ad). These results suggest that net cationic charge of the complex exerts following effects; (1) improves the binding to and subsequent internalization of complex into anionic hMSC and (2) augments gene transfer efficacy of Ad by promoting endosome rupture through proton sponge effect. Additionally, it should be noted that dAd/GFP-PCDP at 1×10^5 molar ratio showed 3-fold lower cytotoxicity (7.4%) compared to dAd/GFP-PEI complex (19.3%, $P < .001$) and induced low level of cytotoxicity that was comparable to those of naked dAd/GFP (Fig. 2B). Altogether, these results show that PCDP polymer is safer than 25 K PEI and that PCDP-mediated loading of oAd into hMSC can overcome poor loading capacity of naked oAd associated with low CAR expression level on surface of these cell carriers.

For further physiochemical characterization of Ad/PCDP complex, the surface charge and particle size of dAd/GFP-PCDP complexes formed at various molar ratios were analyzed by Zetasizer 3000HS. As shown in **Fig. S2**, the average size of naked dAd/GFP was about 103.1 ± 3.7 nm. The complexation of dAd/GFP with PCDP led to polymer concentration-dependent increase in average size between PCDP:Ad molar ratios from 1×10^4 to 2×10^4 (average complex size reached 197.7 ± 28.6 and 311.5 ± 2.0 nm, respectively). Interestingly, the complex size of dAd/GFP-PCDP decreased from 5×10^4 to 1×10^5 in PCDP-dependent manner. TEM imaging was performed to further analyze physical attributes of dAd/GFP-PCDP complex. Increase of PCDP concentration beyond 2×10^4 molar ratio for the generation of dAd/GFP-PCDP complex led to significant molar ratio-dependent decrease in complex diameter (**Fig. S8**; $P < .05$ or .001). These results suggest that increasing PCDP concentration and net cationic charge of Ad-PCDP complex at higher molar ratio either more tightly binds with Ad or condenses the nanocomplex, which is in agreement with our previous publication where higher cationic polymer concentration above threshold level promoted condensation of the nanocomplexes and decrease in average complex diameter [51].

The average surface charge also increased proportionally with size and polymer concentrations (**Fig. S2**); −18.1 ± 2.5 (naked Ad), 15.1 ± 0.8 (PCDP:Ad molar ratio: 1×10^4), and 25.8 ± 0.6 mV (PCDP:Ad molar ratio: 5×10^4). Of note, dAd/GFP-PCDP formed with molar ratio of 1×10^5 (PCDP:Ad) showed significant attenuation in particle size compared to those of complex formed with 1×10^4–5×10^4 molar ratios, resulting in compact size of 148.8 ± 7.8 or 83.3 ± 4.9 nm as determined by DLS or TEM, respectively. Together, these results suggest that PCDP at the molar ratio of 1×10^5 was successfully and stably coated on the surface of Ad through electrostatic interactions. Therefore, based on Fig. 2A and **Fig. S2,** 1×10^5 molar ratio for PCDP:Ad was chosen as an optimal ratio to transduce hMSCs in all subsequent experiments.

3.3. Increased viral production and oncolytic ability of oAd/RLX-PCDP complex in hMSCs

To examine whether enhanced internalization of Ad-PCDP complex into hMSCs could lead to improved viral replication and release, hMSCs were infected with oAd/RLX-PCDP complex, which utilized ECM-degrading oAd expressing RLX (oAd/RLX) and PCDP at PCDP:Ad molar ratio of 1×10 [5]. As shown in Fig. 3A, the total quantity of virions detected from both hMSC and culture supernatant was significantly higher in oAd/RLX-PCDP-loaded hMSCs than those infected with naked oAd/RLX at all MOIs and both time points. In particular, the number of viral particles in the oAd/RLX-PCDP-loaded hMSCs was 83.5- (4 days) to 508.9-fold (8 days) higher than those observed in naked oAd/RLX-loaded hMSCs (5 MOI; $P < .001$), showing that hMSC can serve as a promising Ad delivery platform that is capable of supporting oAd replication. In particular, the highest viral production efficiency was achieved at 5 MOI and viral production level started to plateau at higher virus concentration. This was likely due to rapid cell death and release of virions occurring at higher viral doses, leading to insufficient replication of oAd.

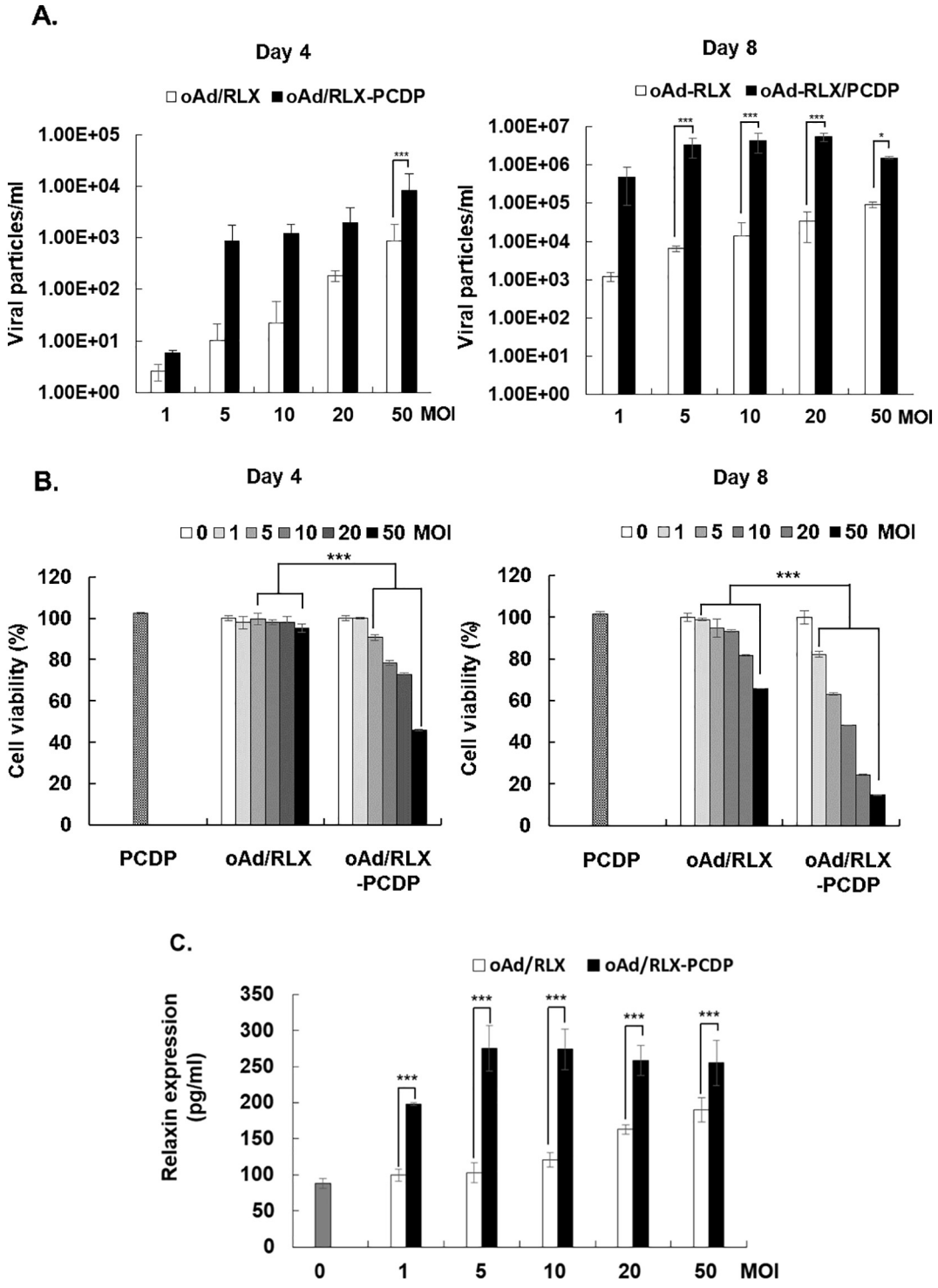

Fig. 3. Viral replication and Relaxin production of oncolytic Ad/RLX-PCDP complex in hMSCs. (A) Viral production by oAd/RLX-PCDP in hMSCs. hMSC cells were infected with naked oAd/RLX, or oAd/RLX-PCDP at various MOIs. After 4 and 8 days post-infection, viral genomic copies was measured by real-time quantitative PCR. (B) Cytotoxicity of oncolytic Ad-PCDP complex in hMSCs. hMSC cells were treated with PCDP, naked oAd/RLX, or oAd/RLX-PCDP at various MOIs. After 4 and 8 days after infection, cell viability was measured by MTT assay. Data presented as mean ± SD. (C) Relaxin expression levels of oAd/RLX-PCDP in hMSCs. hMSC cells were infected with PBS, naked oAd/RLX, or oAd/RLX-PCDP at various MOIs between 0 and 50. Relaxin concentration in the culture supernatant was measured by ELISA assay at 7 days post-infection. The data represent the mean ± SD of triplicates that are representative of 3 independent experiments. $^{*}P < .05$, $^{***}P < .001$ versus naked oAd/RLX.

As optimal cell carrier for oAd should maximize viral production without substantial reduction in cell viability while oAd is delivered to tumor via systemic circulation, we assessed the effect of each formulation on survivability of hMSC at both 4 days and 8 days post-infection. As shown in Fig. 3B, oAd/RLX-PCDP caused significant and dose-dependent reduction in hMSCs viability compared to naked oAd/RLX ($P < .001$). These results suggest that notable reduction in viability of hMSCs by oAd/RLX-PCDP was likely caused by PCDP facilitating the internalization of oAd/RLX into hMSC, thus resulting in greater replication-mediated cytolytic activity in hMSCs (as evidenced

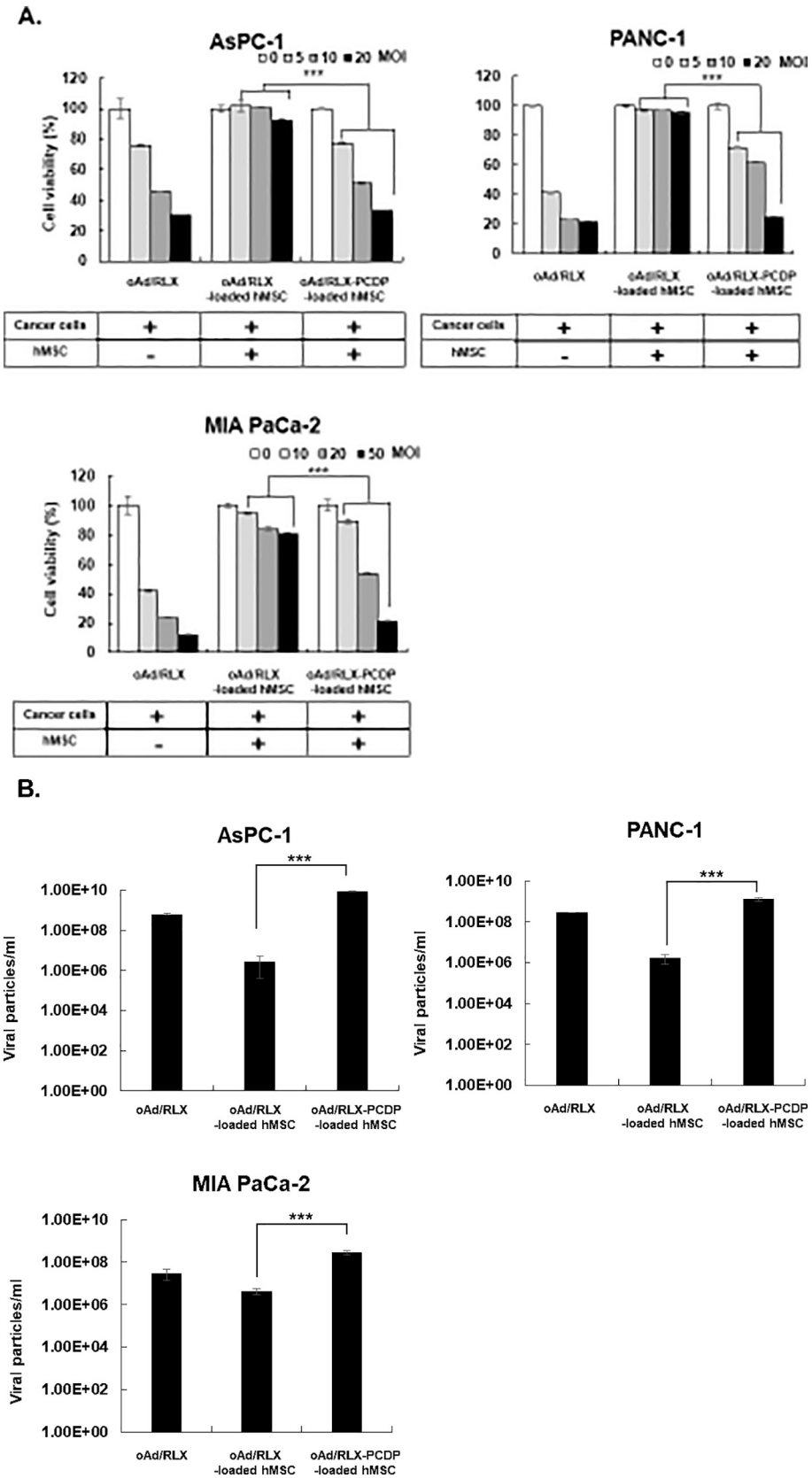

Fig. 4. Cancer cell killing effect and viral replication of oAd/RLX-PCDP complex-loaded hMSCs on various pancreatic cancer cells. (A) Oncolytic effect by PBS, naked oAd/RLX, oAd/RLX-loaded hMSCs, or oAd/RLX-PCDP-loaded hMSCs. Cells (AsPC-1, PANC-1, and MIA PaCa-2) were infected with naked oAd/RLX, oAd/RLX-loaded or oAd/RLX-PCDP-loaded hMSCs at various MOIs. After 4 (AsPC-1 and PANC-1) or 6 (MIA PaCa-2) days post-infection, cell viability was measured by MTT assay. For oAd/RLX groups, the cell viability solely accounts for the absorbance readout of respective cancer cell types. For oAd/RLX- and oAd/RLX-PCDP-loaded hMSC groups, the total cell viability (as determined by absorbance readout) accounts for both respective types of pancreatic cancer cells and surviving hMSC carrier. (B) Viral production. Cells (AsPC-1, PANC-1, and MIA PaCa-2) were infected with naked oAd/RLX, oAd/RLX-loaded hMSCs, or oAd/RLX-PCDP-loaded hMSCs. At 72 h post-infection, viral genomic copies were measured by real-time quantitative PCR. Results represent the mean ± SD of triplicate experiments. ***$P < .001$ versus oAd/RLX-loaded hMSC control.

in Fig. 3A). Of note, both PCDP and naked oAd/RLX treatment (50 MOI at day 4) alone led to insignificant reduction in viability of hMSCs, further supporting our assertion that this effect was caused by superior viral replication rather than any inherent toxicity of these therapeutics. This is claim is further supported by our finding where oAd/RLX-PEI and oAd/RLX-PCDP complex elicits similar level of reduction in the viability of hMSC (**Fig. S3A**), but oAd/RLX-PCDP is the only polymer-coated oncolytic Ad to show significantly higher level of viral

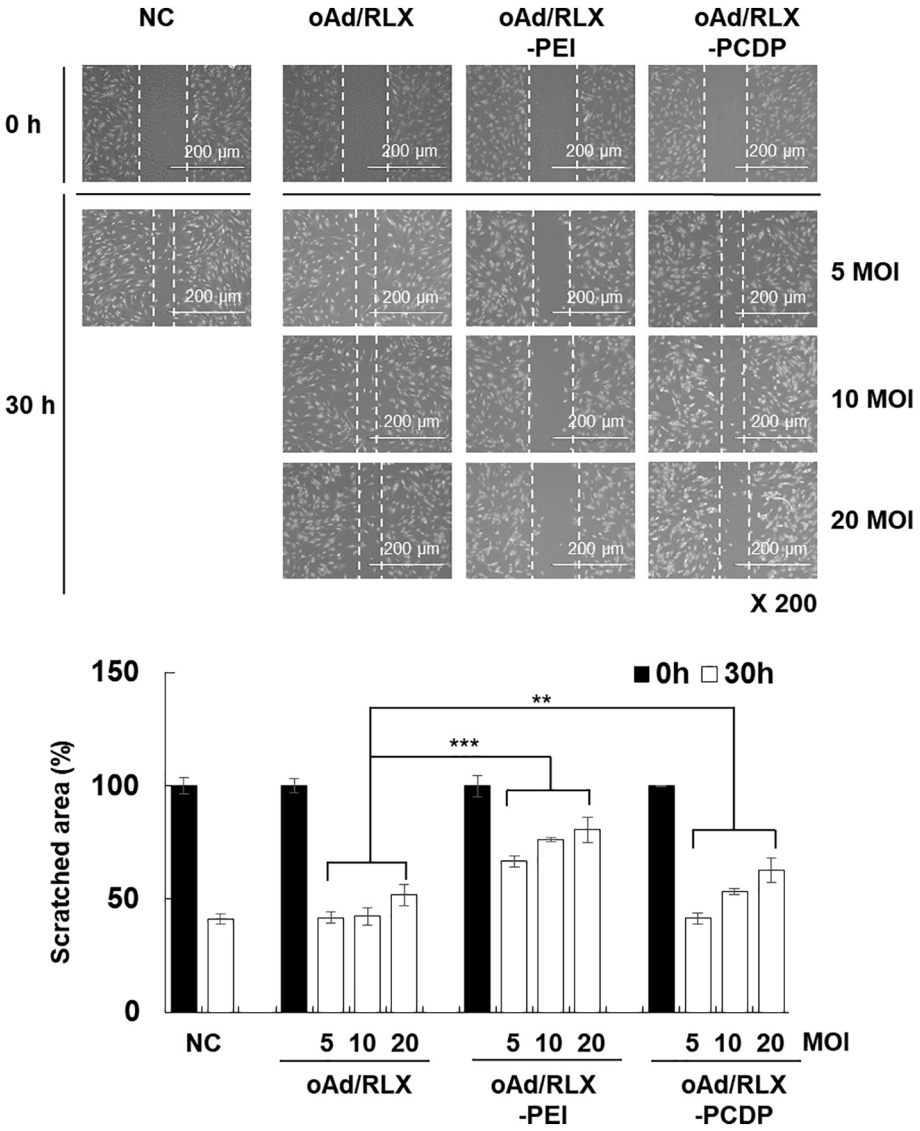

Fig. 5. Effect of oAd/RLX-PCDP complex treatment on the migration capacity of hMSCs. hMSCs were treated with PBS, naked oAd/RLX, oAd/RLX-PEI, or oAd/RLX-PCDP for 18 h at various MOIs. Then, PBS- or oAd-treated hMSCs were scratched with a sterile pipette tip, and cell migration into the scratch was photographed at 0 and 30 h using a microscope. The data represent the mean ± SD of triplicates that are representative of 3 independent experiments. $^{**}P < .01$, $^{***}P < .001$ versus oAd/RLX.

production than naked oAd/RLX (**Fig. S3B**). These results suggest that PCDP enables efficient cellular internalization of oAd into hMSC without significant cytotoxicity (as observed by 25 K PEI) to allow effective viral replication in the cell carrier.

Based on these results, we identified that 5 MOI of oAd/RLX is the optimal dose for hMSCs as highest level of viral production was achieved with minimal reduction in hMSC viability. These attributes are important to achieve maximum therapeutic efficacy with oAd-loaded cell carriers as systemically administered carriers must survive long enough to deliver oAd to tumor tissues while permitting the virions to efficiently replicate.

In line with viral production results, RLX ELISA revealed that oAd/RLX-PCDP induced significantly higher RLX expression level across all viral doses than naked oAd/RLX ($P < .001$, Fig. 3C). These results suggest that the complexation of oAd with PCDP leads to more efficient viral replication and transgene expressions in hMSCs.

3.4. Cancer cell killing profile of oAd/RLX-PCDP-loaded hMSCs

To assess the ability of oAd-loaded hMSCs as a therapeutic tool for pancreatic cancer treatment, cancer cell killing effects of oAd/RLX-PCDP loaded in hMSCs were verified using MTT assay against pancreatic cancer cells (AsPC-1, PANC-1 and MIA PaCa-2) (Fig. 4A). The hMSCs were treated with PBS, naked oAd/RLX, or oAd/RLX-PCDP complex at different MOIs for 18 h, then the cells were detached, and then co-incubated with pre-seeded pancreatic cancer cells. Naked oAd/RLX as a control was infected into the pancreatic cancer cell lines at the same dosage to show the original susceptibility of pancreatic cancer cells to oAd/RLX. As shown in Fig. 4A, naked oAd/RLX showed potent cancer cell killing efficacy in all cancer cell lines in a dose-dependent manner, killing 69.5% of AsPC-1 cells, 77.5% of PANC-1 cells and 87.6% of MIA PaCa-2 cells at highest respective viral doses. In marked contrast, the treatment of naked oAd/RLX with hMSC carrier had significantly reduced oncolytic efficacy due to the low transduction efficiency, resulting in cell killing of 7.6% for AsPC-1 cells, 4.1% for PANC-1, and 18.4% for MIA PaCa-2 at the same MOI as naked oAd control. Unlike oAd/RLX-loaded hMSC group, oAd/RLX-PCDP-loaded hMSC treatment elicited potent cancer cell killing effect that was comparable to those of naked oAd/RLX at the highest viral doses; 76.7% (AsPC-1 cells), 74.3% (PANC-1 cells), and 78.4% (MIA Paca-2 cells) cell killing

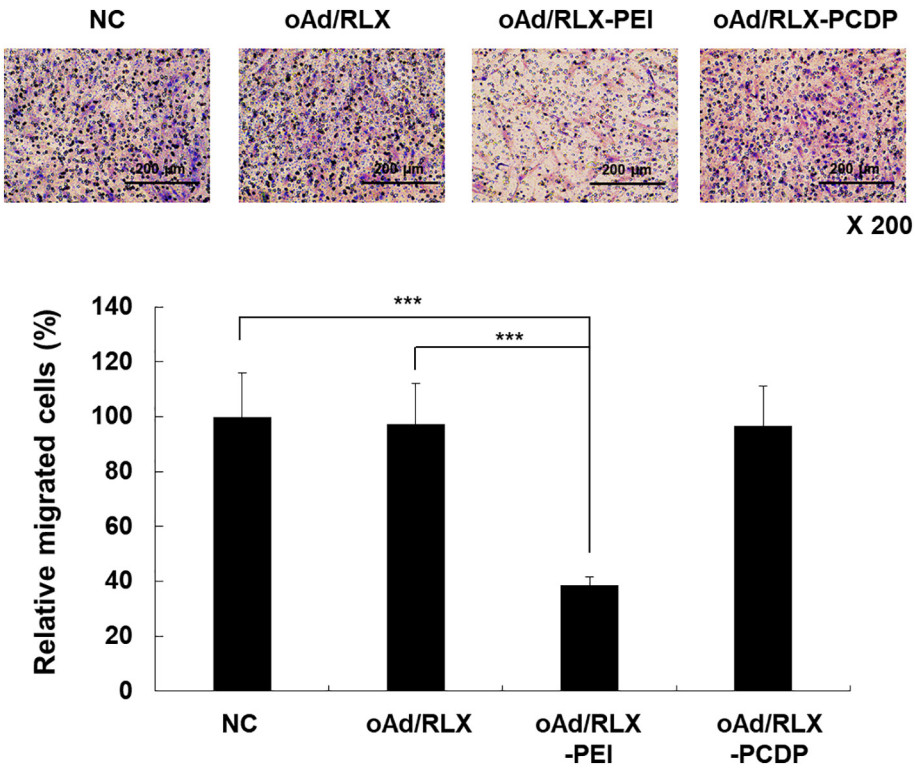

Fig. 6. Tumor-tropic migratory properties of oAd/RLX-PCDP complex-loaded hMSCs. oAd/RLX, oAd/RLX-PEI, and oAd/RLX-PCDP complex were treated into hMSCs at 5 MOI. After 18 h, these cells were detached and co-cultured with pancreatic cancer cells (AsPC-1) into the transwell plate for 30 h. Then, the migrated cells were fixed and stained with hematoxylin and eosin solution. All conditions were done in quadruplicate and repeated in two separate experiments. ***$P < .001$ versus uninfected hMSC (negative control) or naked oAd/RLX.

effect, which was 10.1-, 18.1- and 4.3-fold greater cancer cell killing efficacy than oAd/RLX-loaded hMSCs group, respectively ($P < .001$). Interestingly, hMSC treated with either 25 K PEI- or PCDP-coated virus showed similar level of reduction in hMSC viability (**Fig. S3A**). However, the viral replication within hMSC was 3.9-fold higher following treatment with oAd/RLX-PCDP in comparison to those treated with oAd/RLX-PEI (**Fig. S3B**). These findings suggest that reduction in hMSC viability following infection with 25 K PEI-coated virus was not viral replication-mediated cytopathic effect and rather it was mediated by high level of polymer toxicity. The comparison of naked oAd/RLX and oAd/RLX-PEI further support this claim as naked oAd/RLX, which cannot internalize efficiently into hMSC due to low expression level of CAR, elicited no observable cytopathic effect on hMSC while it exhibited similar level of viral particles as oAd/RLX-PEI group. In specific, oAd/RLX-PCDP-loaded hMSC showed 13.9-, 4.5-, and 9.7-fold greater viral particles than that of naked oAd and 3246.1-, 114.7-, and 65.7-fold higher viral yield compared to oAd/RLX-loaded hMSC, respectively ($P < .001$). Together, these results suggest that hMSC-mediated delivery of oAd/RLX-PCDP may facilitate replication of oAd in pancreatic cancer cells.

3.5. *In vitro migratory characteristics of oAd-PCDP complex-loaded hMSCs*

The strength of hMSCs as a carrier in cancer therapy is their tumor homing ability [52]. Thus, we assessed whether oAd-loaded hMSCs retained their ability to migrate by wound healing assay. As shown in Fig. 5, the wound closure ratios in all treatment groups decreased with increasing viral dose. The virus-dependent wound closure was least evident in naked oAd-treated cells where the migration profile was similar among all tested viral doses, likely due to poor susceptibility of hMSC to Ad infection. On the other hand, PEI-coated oAd-loaded hMSCs showed the lowest migration ability in comparison to other groups. Importantly, oAd/RLX-PCDP-loaded cells at 5 MOI showed similar wound healing ability compared to negative control or naked oAd-treated cells; 58.8%, 58.2%, and 58.5% for hMSCs in the negative control (PBS) group, naked oAd/RLX, and oAd/RLX-PCDP at 5 MOI, respectively. Neither free PEI nor PCDP affected the wound closing capacity hMSC, suggesting that the combination of both polymer and oAd/RLX into a nanocomplex is necessary to affect hMSC wound healing capacity (**Fig. S7**). These results suggest that oAd/RLX-PCDP-loaded hMSCs at 5 MOI did not lose their original migration capacity. Furthermore, these optimization results are in good agreement with our findings from previous figures and thus these conditions were employed for the generation of oAd/RLX-PCDP-loaded hMSCs in all of our subsequent experiments.

Next, we assessed whether oAd/RLX-PCDP-loaded hMSCs could migrate toward pancreatic cancer cells in vitro. The migration ability of hMSCs to cancer cells was examined in a co-culture system using a two-chamber slide in which hMSCs were seeded on the upper chamber while the pancreatic cancer cells (AsPC-1) were seeded on the lower chamber. As shown in Fig. 6, oAd/RLX-PEI-loaded hMSCs showed significantly poorer migration capability to pancreatic cancer cells compared to naked oAd/RLX- or oAd/RLX-PCDP-loaded hMSCs, suggesting that toxicity of PEI may deteriorate tumor homing ability of hMSCs ($P < .001$). Importantly, oAd/RLX-PCDP-loaded hMSCs showed similar tumor homing ability as those of untreated hMSCs, showing that PCDP, unlike PEI 25 K, did not damage the hMSC and restrict the migration ability of hMSCs to cancer cells. Taken together, these findings indicate that the treatment of oAd/RLX-PCDP into hMSCs did not exert negative effects on hMSC's natural ability to migrate to cancer cells.

3.6. *Enhanced therapeutic efficacy of oAd-PCDP complex-loaded hMSCs in tumor-bearing mice*

To confirm the therapeutic potential of the oAd/RLX-PCDP-loaded hMSCs in vivo, AsPC-1 subcutaneous tumor-bearing mice were intravenously injected 3 times with PBS, PCDP polymer, hMSCs, naked oAd/RLX, oAd/RLX-loaded hMSCs, or oAd/RLX-PCDP-loaded hMSCs. For each injection, 1×10^6 hMSCs were utilized as reported previously [41,52] and the viral dose infected into hMSCs was decided to 5 MOI (5×10^8 VP/injection) based on in vitro results (Figs. 5 and 6). As shown in Fig. 7A, systemic treatment with oAd/RLX-PCDP-loaded hMSCs resulted in significantly higher antitumor effect than naked oAd/RLX, oAd/RLX-loaded hMSC, or other control groups. At 21 days

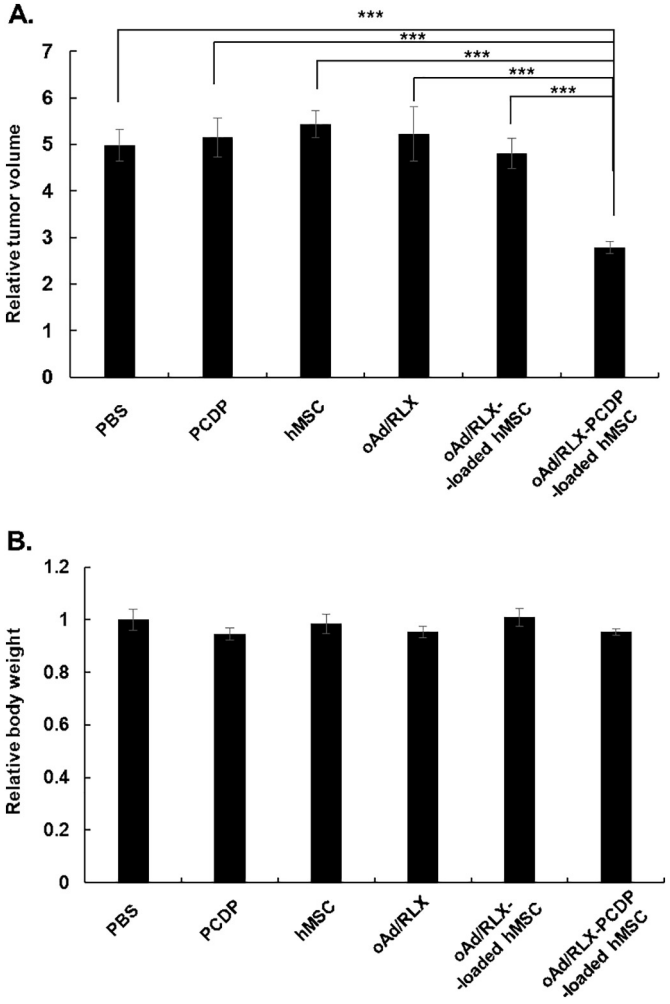

Fig. 7. In vivo antitumor efficacy of oAd/RLX-PCDP-loaded hMSCs in tumor-bearing mice. Pancreatic tumor xenograft model was established by injecting AsPC-1 cells (5×10^6) subcutaneously in nude mice ($n = 8$). Following the confirmation of tumorigenesis, the treatments were systemically administered on 4 day intervals for total of 3 injections when the average tumor volumes reached 90 mm^3. (A) Relative tumor volume of each treatment group at day 21 post treatment in respect to initial tumor volume from day 1. (B) Relative body weight of each treatment group in respect to PBS treatment group at 21 days post initial treatment. (C) Histological and immunohistochemical analysis of tumor tissues from mice treated with PBS, PCDP, hMSC, naked oAd/RLX, oAd/RLX-loaded hMSC, or oAd/RLX-PCDP-loaded hMSC. Tumor tissues were collected from mice at 3 days after the final treatment. Representative sections were stained with H & E or MT solution. TUNEL assay was performed to detect apoptosis, and the expression of E1A was assessed by immunohistochemistry. Data presented as mean ± SD. ***$P < .001$ versus PBS, PCDP, hMSC, naked oAd/RLX, and oAd/RLX-loaded hMSC.

post-injection, all treatment groups except oAd/RLX-PCDP-loaded hMSC group exhibited 4.8-fold or greater increase in tumor volume when compared with average tumor volume of respective group on day 1 of treatment. In marked contrast, the volume of oAd/RLX-PCDP-loaded hMSCs-treated tumors were only increased by 2.8-fold on day 21 compared to day 1 of treatment, showing 42.1 to 48.9% more potent tumor tumor growth inhibiting activity than any other treatment ($P < .001$). All treatment groups did not show significant weight loss in mice, illustrating the good safety profile of both oAd/RLX, hMSC, and polymeric carriers (Fig. 7B).

Next, to further investigate the therapeutic efficacy of oAd/RLX-PCDP-loaded hMSC carriers, tumor tissues were harvested at 3 days after the final treatment and then analyzed histologically and immunohistochemically. As shown in Fig. 7C, H & E staining revealed large areas of extensive necrosis in the tumor tissue treated with oAd/RLX-PCDP-loaded hMSC carrier. Masson's trichrome (MT) staining revealed that tissue treated with oAd/RLX-PCDP-loaded hMSC group resulted in markedly lower level of collagen compared to the tissues treated with other groups. This was likely due to more effective trafficking of oAd/RLX to tumor tissues by oAd/RLX-PCDP-loaded hMSC treatment group than others as evidenced by highest level of Ad E1A in these tissues, suggesting that efficient delivery of oAd/RLX to tumor tissues and subsequent expression of RLX led to degradation of tumor ECM. These results are consistent with previous studies that the tumors treated with RLX-expressing Ad showed highly reduced collagen [26].

Importantly, it should be noted that there was no Ad E1A detectable in either oAd- or oAd-loaded hMSC-treated mice, showing that naked virus or poor loading of virus into hMSC will severely restrict intratumoral accumulation of oAd. TUNEL assay also showed similar results as E1A staining in the tumor of the oAd/RLX-PCDP-loaded hMSC group, showing the largest apoptotic proportion of cancer cells. Of note, naked oAd/RLX did not show potent in vivo antitumor effect compared to oAd/RLX-PCDP-loaded hMSC group even though they displayed potent in vitro cancer cell killing efficacy with effective viral replication as in Fig. 4. Based on the previous studies to show antitumor effects by systemically injected naked oAd, we speculate that the amount of naked oAd used in this study (5×10^8 VP/injection) was not enough to localize to the target tumor sites and induce cancer-killing effect into the tumors [3]. In the case of oAd/RLX-loaded hMSC group, poor therapeutic efficacy in vivo mice model was consistent with the lower transduction and viral production efficiency of oAd into the hMSC in vitro (Fig. 3). Further, biodistribution profiling studies evaluating hMSC and oAd accumulation in several organs at 24 h after systemic administration revealed that hMSC was detected at a highest level in the lungs following systemic administration of hMSC alone (**Fig. S6A**; $P < .001$ versus oAd/RLX-loaded hMSC or oAd/RLX-PCDP-loaded hMSC), which is in agreement with publication by others similarly demonstrating the early and large portion of systemically administered hMSC accumulating in the lungs [53]. In contrast, hMSC was observed at a level close to the detection limit in the lungs following systemic administration of oAd/RLX- and oAd/RLX-PCDP-loaded hMSCs. Despite negligible level of hMSC being observed in the lungs following systemic administration of oAd/RLX- or oAd/RLX-PCDP-loaded hMSCs, higher quantity of oAd was detected in the lung tissues by these groups than naked oAd/RLX (**Fig. S6B**; $P < .001$). These results suggest that loading of oAd/RLX or oAd/RLX-PCDP into hMSC promotes oAd accumulation in the lungs, likely due to the lung tropism of hMSC. Additionally, oAd/RLX was accumulated at a significant higher level in the lung tissues following treatment with oAd/RLX-PCDP-loaded hMSC in comparison with oAd/RLX-loaded hMSC ($P < .001$). This result indicates that more efficient cell uptake (**Fig. S4**) and viral replication (Fig. 3A) by oAd/RLX-PCDP (compared to naked oAd/RLX) into and within hMSC, respectively, can augment systemic oAd delivery efficiency using hMSC carrier. Notably, we did not observe hepatic accumulation of oAd following systemic administration of naked oAd/RLX, despite previously reported hepatic tropism of systemically administered Ad [54,55]. This was likely due to naked oAd/RLX being administered at 400-fold lower dose via single injection in respect to frequently reported systemic oAd dose (2×10^{10} VP and 2–3 total injections [9,56,57]). Further, loading of oAd/RLX or oAd/RLX-PCDP into hMSC also promotes the rapid removal of hMSC from the host system within 24 h of systemic administration, since efficient replication of oAd/RLX in hMSC (as shown in Fig. 3A) would destroy hMSC via cytolysis. Timely removal of hMSC from host is critical to abrogate any potential side effect that may arise from unintended engraftment of hMSC to host tissues; poorly regulated stem cell therapeutics may promote oncogenesis and this remains a major clinical hurdle of all stem cell-based therapeutics [57–59]. Taken together, these results suggest that oAd/RLX-PCDP-loaded hMSC carrier can be delivered efficiently to target tumor tissues after systemic injection

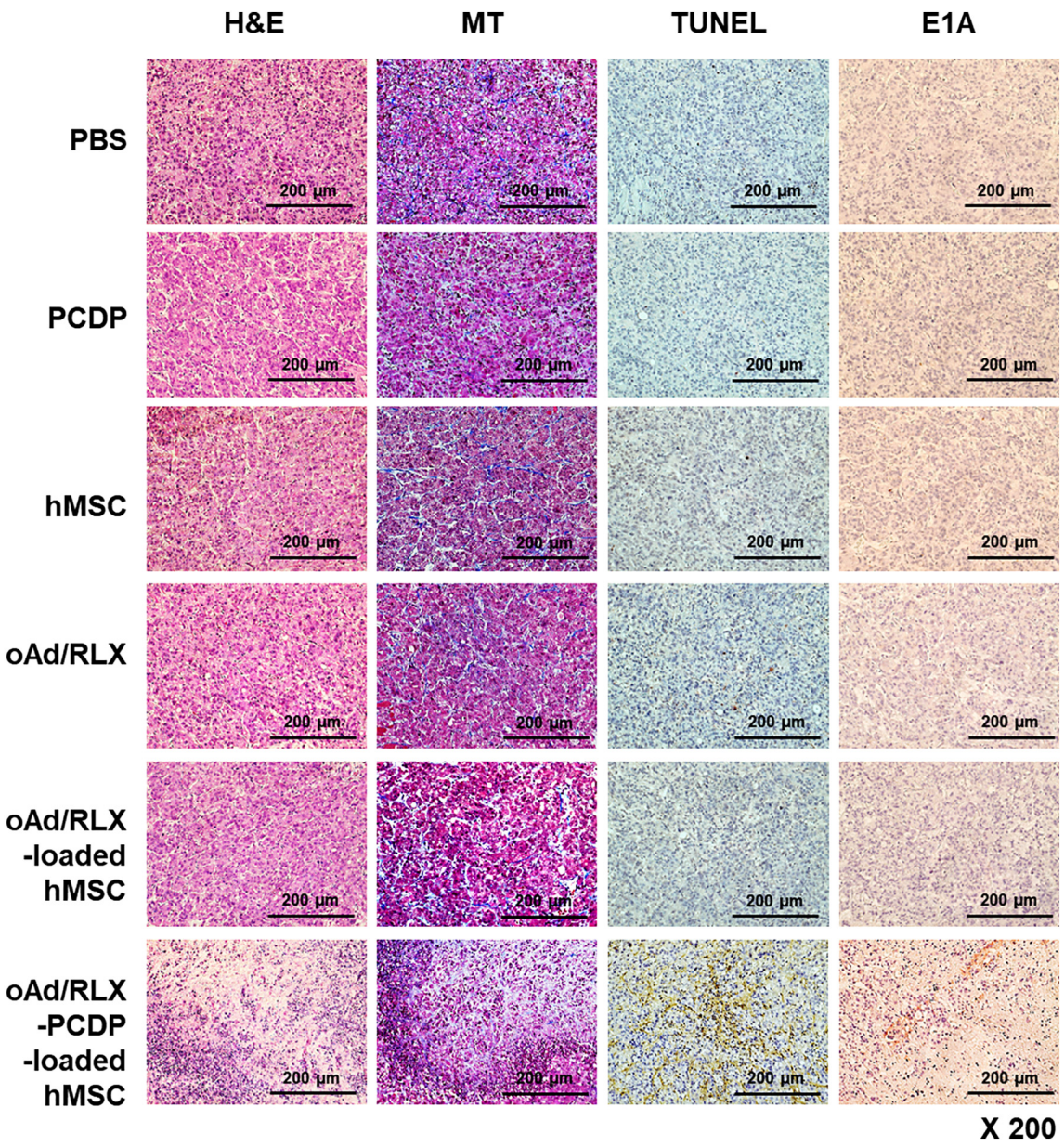

Fig. 7. (*continued*)

where it induces effective viral replication and RLX expression, resulting in enhanced antitumor efficacy.

4. Conclusions

Although tumor homing ability of hMSCs makes it a promising candidate to systemically deliver oncolytic viruses to tumor tissues, conventional oAd cannot be efficiently loaded into hMSCs due to low surface expression of CAR in hMSCs. Our findings show that loading efficiency of oAd into hMSCs can be greatly enhanced by complexing the oAd with cationic polymer PCDP. Unlike conventional cationic polymer, PCDP-mediated loading of oAd was minimally detrimental to hMSCs and their tumor homing ability. PCDP-mediated internalization of oAd led to improved therapeutic gene expression and viral replication in vitro. Similar results were evidenced in vivo where systemic delivery oAd at relatively low viral dose with PCDP and hMSC led to efficient accumulation and replication of oAd at tumor tissues, ultimately leading to potent tumor growth inhibition by induction of apoptotic cell death and degradation of tumor ECM. Taken together, these results suggest that oAd/RLX-PCDP-loaded hMSC therapy is applicable as one of the highly promising tools for effective systemic oncolytic virotherapy to treat pancreatic cancer.

Acknowledgements

This work was supported by grants from the National Institutes of Health, USA (CA177932) to Dr. SW. KIM. Additional supports were provided by grants from the National Research Foundation of Korea to Dr. Chae-Ok Yun (2016M3A9B5942352). We are grateful to Pharmicell Co.Ltd., Sungnam, South Korea, for providing hMSCs from a healthy donor.

Appendix A. Supplementary data

Supplementary data to this article can be found online at https://doi.org/10.1016/j.jconrel.2019.04.040.

References

[1] M. Jiang, Z. Liu, Y. Xiang, H. Ma, S. Liu, Y. Liu, D. Zheng, Synergistic antitumor effect of AAV-mediated TRAIL expression combined with cisplatin on head and neck squamous cell carcinoma, BMC Cancer 11 (2011) 54.

[2] J.W. Choi, Y.S. Lee, C.O. Yun, S.W. Kim, Polymeric oncolytic adenovirus for cancer gene therapy, J. Control. Release Off. J. Control. Release Soc 219 (2015) 181–191.

[3] J. Hong, C.O. Yun, Emergence of ad-mediated combination therapy against cancer: what to expect? Current Cancer Drug Targets, vol. 18, 2018, pp. 139–152.

[4] A.R. Yoon, J. Hong, S.W. Kim, C.O. Yun, Redirecting adenovirus tropism by genetic, chemical, and mechanical modification of the adenovirus surface for cancer gene therapy, Expert Opin. Drug Deliv 13 (2016) 843–858.

[5] J.W. Choi, J.S. Lee, S.W. Kim, C.O. Yun, Evolution of oncolytic adenovirus for cancer treatment, Adv. Drug Deliv. Rev. 64 (2012) 720–729.

[6] P.H. Kim, J.H. Sohn, J.W. Choi, Y. Jung, S.W. Kim, S. Haam, C.O. Yun, Active targeting and safety profile of PEG-modified adenovirus conjugated with herceptin, Biomaterials 32 (2011) 2314–2326.

[7] D. Kasala, A.R. Yoon, J. Hong, S.W. Kim, C.O. Yun, Evolving lessons on nanomaterial-coated viral vectors for local and systemic gene therapy, Nanomedicine 11 (2016) 1689–1713.

[8] B.K. Jung, E. Oh, J. Hong, Y. Lee, K.D. Park, C.O. Yun, A hydrogel matrix prolongs persistence and promotes specific localization of an oncolytic adenovirus in a tumor by restricting nonspecific shedding and an antiviral immune response, Biomaterials 147 (2017) 26–38.

[9] D. Kasala, S.H. Lee, J.W. Hong, J.W. Choi, K. Nam, Y.H. Chung, S.W. Kim, C.O. Yun, Synergistic antitumor effect mediated by a paclitaxel-conjugated polymeric micelle-coated oncolytic adenovirus, Biomaterials 145 (2017) 207–222.

[10] O.J. Kwon, E. Kang, S. Kim, C.O. Yun, Viral genome DNA/lipoplexes elicit in situ oncolytic viral replication and potent antitumor efficacy via systemic delivery, J. Control. Release Off. J. Control. Release Soc 155 (2011) 317–325.

[11] C. Willmon, K. Harrington, T. Kottke, R. Prestwich, A. Melcher, R. Vile, Cell carriers for oncolytic viruses: Fed Ex for cancer therapy, Mol. Ther. J. Am. Soc. Gene Ther 17 (2009) 1667–1676.

[12] E.K. Sage, R.M. Thakrar, S.M. Janes, Genetically modified mesenchymal stromal cells in cancer therapy, Cytotherapy 18 (2016) 1435–1445.

[13] S. Schu, M. Nosov, L. O'Flynn, G. Shaw, O. Treacy, F. Barry, M. Murphy, T. O'Brien, T. Ritter, Immunogenicity of allogeneic mesenchymal stem cells, J. Cell. Mol. Med. 16 (2012) 2094–2103.

[14] R.M. Dwyer, M.J. Kerin, Mesenchymal stem cells and cancer: tumor-specific delivery vehicles or therapeutic targets? Hum. Gene Ther. 21 (2010) 1506–1512.

[15] Y.L. Hu, Y.H. Fu, Y. Tabata, J.Q. Gao, Mesenchymal stem cells: a promising targeted-delivery vehicle in cancer gene therapy, J. Control. Release Off. J. Control. Release Soc 147 (2010) 154–162.

[16] A. Nakamizo, F. Marini, T. Amano, A. Khan, M. Studeny, J. Gumin, J. Chen, S. Hentschel, G. Vecil, J. Dembinski, M. Andreeff, F.F. Lang, Human bone marrow-derived mesenchymal stem cells in the treatment of gliomas, Cancer Res. 65 (2005) 3307–3318.

[17] R.M. Dwyer, J. Ryan, R.J. Havelin, J.C. Morris, B.W. Miller, Z. Liu, R. Flavin, C. O'Flatharta, M.J. Foley, H.H. Barrett, J.M. Murphy, F.P. Barry, T. O'Brien, M.J. Kerin, Mesenchymal stem cell-mediated delivery of the sodium iodide symporter supports radionuclide imaging and treatment of breast cancer, Stem Cells 29 (2011) 1149–1157.

[18] D. van Poll, B. Parekkadan, C.H. Cho, F. Berthiaume, Y. Nahmias, A.W. Tilles, M.L. Yarmush, Mesenchymal stem cell-derived molecules directly modulate hepatocellular death and regeneration in vitro and in vivo, Hepatology 47 (2008) 1634–1643.

[19] N. Serakinci, R. Christensen, U. Fahrioglu, F.B. Sorensen, F. Dagnaes-Hansen, M. Hajek, T.H. Jensen, S. Kolvraa, N.W. Keith, Mesenchymal stem cells as therapeutic delivery vehicles targeting tumor stroma, Cancer Biother. Radiopharm. 26 (2011) 767–773.

[20] E.K. Mader, Y. Maeyama, Y. Lin, G.W. Butler, H.M. Russell, E. Galanis, S.J. Russell, A.B. Dietz, K.W. Peng, Mesenchymal stem cell carriers protect oncolytic measles viruses from antibody neutralization in an orthotopic ovarian cancer therapy model, Clin. Cancer Res. Off. J. Am. Assoc. Cancer Res 15 (2009) 7246–7255.

[21] J.L. Dembinski, E.L. Spaeth, J. Fueyo, C. Gomez-Manzano, M. Studeny, M. Andreeff, F.C. Marini, Reduction of nontarget infection and systemic toxicity by targeted delivery of conditionally replicating viruses transported in mesenchymal stem cells, Cancer Gene Ther. 17 (2010) 289–297.

[22] A.M. Sonabend, I.V. Ulasov, M.A. Tyler, A.A. Rivera, J.M. Mathis, M.S. Lesniak, Mesenchymal stem cells effectively deliver an oncolytic adenovirus to intracranial glioma, Stem Cells 26 (2008) 831–841.

[23] L. Pereboeva, S. Komarova, G. Mikheeva, V. Krasnykh, D.T. Curiel, Approaches to utilize mesenchymal progenitor cells as cellular vehicles, Stem Cells 21 (2003) 389–404.

[24] P.A. Conget, J.J. Minguell, Adenoviral-mediated gene transfer into ex vivo expanded human bone marrow mesenchymal progenitor cells, Exp. Hematol. 28 (2000) 382–390.

[25] K. Hammer, A. Kazcorowski, L. Liu, M. Behr, P. Schemmer, I. Herr, D.M. Nettelbeck, Engineered adenoviruses combine enhanced oncolysis with improved virus production by mesenchymal stromal carrier cells, Int. J. Cancer 137 (2015) 978–990.

[26] I. Dmitriev, V. Krasnykh, C.R. Miller, M. Wang, E. Kashentseva, G. Mikheeva, N. Belousova, D.T. Curiel, An adenovirus vector with genetically modified fibers demonstrates expanded tropism via utilization of a coxsackievirus and adenovirus receptor-independent cell entry mechanism, J. Virol. 72 (1998) 9706–9713.

[27] V.N. Krasnykh, G.V. Mikheeva, J.T. Douglas, D.T. Curiel, Generation of recombinant adenovirus vectors with modified fibers for altering viral tropism, J. Virol. 70 (1996) 6839–6846.

[28] J. Garcia-Castro, R. Alemany, M. Cascallo, J. Martinez-Quintanilla, M. Arriero Mdel, A. Lassaletta, L. Madero, M. Ramirez, Treatment of metastatic neuroblastoma with systemic oncolytic virotherapy delivered by autologous mesenchymal stem cells: an exploratory study, Cancer Gene Ther. 17 (2010) 476–483.

[29] E. Rincon, T. Cejalvo, D. Kanojia, A. Alfranca, M.A. Rodriguez-Milla, R.A. Gil Hoyos, Y. Han, L. Zhang, R. Alemany, M.S. Lesniak, J. Garcia-Castro, Mesenchymal stem cell carriers enhance antitumor efficacy of oncolytic adenoviruses in an immunocompetent mouse model, Oncotarget 8 (2017) 45415–45431.

[30] S. Li, J. Chen, H. Xu, J. Long, X. Xie, Y. Zhang, The targeted transduction of MMP-overexpressing tumor cells by ACPP-HPMA copolymer-coated adenovirus conjugates, PLoS One 9 (2014) e100670.

[31] R. Carlisle, J. Choi, M. Bazan-Peregrino, R. Laga, V. Subr, L. Kostka, K. Ulbrich, C.C. Coussios, L.W. Seymour, Enhanced tumor uptake and penetration of virotherapy using polymer stealthing and focused ultrasound, J. Natl. Cancer Inst. 105 (2013) 1701–1710.

[32] G.K. Grunwald, A. Vetter, K. Klutz, M.J. Willhauck, N. Schwenk, R. Senekowitsch-Schmidtke, M. Schwaiger, C. Zach, E. Wagner, B. Goke, P.S. Holm, M. Ogris, C. Spitzweg, EGFR-targeted adenovirus Dendrimer coating for improved systemic delivery of the Theranostic NIS gene, Mol. Ther. Nucleic Acids 2 (2013) e131.

[33] F. Jonsson, C. Hagedorn, F. Kreppel, Combined genetic and chemical capsid modifications of adenovirus-based gene transfer vectors for shielding and targeting, J. Vis. Exp 140 (2018), https://doi.org/10.3791/58480 e58480, 10 pages.

[34] J.P. Nam, S. Kim, S.W. Kim, Design of PEI-conjugated bio-reducible polymer for efficient gene delivery, Int. J. Pharm. 545 (2018) 295–305.

[35] J.H. Kim, Y.S. Lee, H. Kim, J.H. Huang, A.R. Yoon, C.O. Yun, Relaxin expression from tumor-targeting adenoviruses and its intratumoral spread, apoptosis induction, and efficacy, J. Natl. Cancer Inst. 98 (2006) 1482–1493.

[36] W.J. Lee, Y.O. Kim, I.K. Choi, D.K. Rah, C.O. Yun, Adenovirus-relaxin gene therapy for keloids: implication for reversing pathological fibrosis, Br. J. Dermatol. 165 (2011) 673–677.

[37] H. Kim, K. Nam, J.P. Nam, H.S. Kim, Y.M. Kim, W.S. Joo, S.W. Kim, VEGF therapeutic gene delivery using dendrimer type bio-reducible polymer into human mesenchymal stem cells (hMSCs), J. Control. Release Off. J. Control. Release Soc 220 (2015) 222–228.

[38] M. Ou, X.L. Wang, R. Xu, C.W. Chang, D.A. Bull, S.W. Kim, Novel biodegradable poly(disulfide amine)s for gene delivery with high efficiency and low cytotoxicity, Bioconjug. Chem. 19 (2008) 626–633.

[39] S. Leitner, K. Sweeney, D. Oberg, D. Davies, E. Miranda, N.R. Lemoine, G. Hallden, Oncolytic adenoviral mutants with E1B19K gene deletions enhance gemcitabine-induced apoptosis in pancreatic carcinoma cells and anti-tumor efficacy in vivo, Clin. Cancer Res. Off. J. Am. Assoc. Cancer Res 15 (2009) 1730–1740.

[40] O.J. Kwon, E. Kang, J.W. Choi, S.W. Kim, C.O. Yun, Therapeutic targeting of chitosan-PEG-folate-complexed oncolytic adenovirus for active and systemic cancer gene therapy, J. Control. Release Off. J. Control. Release Soc 169 (2013) 257–265.

[41] M.A. Stoff-Khalili, A.A. Rivera, J.M. Mathis, N.S. Banerjee, A.S. Moon, A. Hess, R.P. Rocconi, T.M. Numnum, M. Everts, L.T. Chow, J.T. Douglas, G.P. Siegal, Z.B. Zhu, H.G. Bender, P. Dall, A. Stoff, L. Pereboeva, D.T. Curiel, Mesenchymal stem cells as a vehicle for targeted delivery of CRAds to lung metastases of breast carcinoma, Breast Cancer Res Treat 105 (2007) 157–167.

[42] H. Xin, M. Kanehira, H. Mizuguchi, T. Hayakawa, T. Kikuchi, T. Nukiwa, Y. Saijo, Targeted delivery of CX3CL1 to multiple lung tumors by mesenchymal stem cells, Stem Cells 25 (2007) 1618–1626.

[43] M.R. Loebinger, A. Eddaoudi, D. Davies, S.M. Janes, Mesenchymal stem cell delivery of TRAIL can eliminate metastatic cancer, Cancer Res. 69 (2009) 4134–4142.

[44] M. Creane, L. Howard, T. O'Brien, C.M. Coleman, Biodistribution and retention of locally administered human mesenchymal stromal cells: quantitative polymerase chain reaction-based detection of human DNA in murine organs, Cytotherapy 19 (2017) 384–394.

[45] M. Studeny, F.C. Marini, R.E. Champlin, C. Zompetta, I.J. Fidler, M. Andreeff, Bone marrow-derived mesenchymal stem cells as vehicles for interferon-beta delivery into tumors, Cancer Res. 62 (2002) 3603–3608.

[46] S. Komarova, Y. Kawakami, M.A. Stoff-Khalili, D.T. Curiel, L. Pereboeva, Mesenchymal progenitor cells as cellular vehicles for delivery of oncolytic adenoviruses, Mol. Cancer Ther. 5 (2006) 755–766.

[47] T. Hakkarainen, M. Sarkioja, P. Lehenkari, S. Miettinen, T. Ylikomi, R. Suuronen, R.A. Desmond, A. Kanerva, A. Hemminki, Human mesenchymal stem cells lack tumor tropism but enhance the antitumor activity of oncolytic adenoviruses in orthotopic lung and breast tumors, Hum. Gene Ther. 18 (2007) 627–641.

[48] D. Putnam, C.A. Gentry, D.W. Pack, R. Langer, Polymer-based gene delivery with low cytotoxicity by a unique balance of side-chain termini, Proc. Natl. Acad. Sci. U. S. A. 98 (2001) 1200–1205.

[49] H. Song, G. Wang, B. He, L. Li, C. Li, Y. Lai, X. Xu, Z. Gu, Cationic lipid-coated PEI/DNA polyplexes with improved efficiency and reduced cytotoxicity for gene delivery into mesenchymal stem cells, Int. J. Nanomedicine 7 (2012) 4637–4648.

[50] S.J. Jung, D. Kasala, J.W. Choi, S.H. Lee, J.K. Hwang, S.W. Kim, C.O. Yun, Safety profiles and antitumor efficacy of oncolytic adenovirus coated with bioreducible polymer in the treatment of a CAR negative tumor model, Biomacromolecules 16 (2015) 87–96.

[51] J.W. Choi, J. Kim, Q.N. Bui, Y. Li, C.O. Yun, D.S. Lee, S.W. Kim, Tuning surface charge and PEGylation of biocompatible polymers for efficient delivery of nucleic acid or adenoviral vector, Bioconjug. Chem. 26 (2015) 1818–1829.

[52] X. Xia, T. Ji, P. Chen, X. Li, Y. Fang, Q. Gao, S. Liao, L. You, H. Xu, Q. Ma, P. Wu, W. Hu, M. Wu, L. Cao, K. Li, Y. Weng, Z. Han, J. Wei, R. Liu, S. Wang, G. Xu, D. Wang, J. Zhou, D. Ma, Mesenchymal stem cells as carriers and amplifiers in CRAd

delivery to tumors, Mol. Cancer 10 (2011) 134.
[53] J. Leibacher, R. Henschler, Biodistribution, migration and homing of systemically applied mesenchymal stem/stromal cells, Stem Cell Res Ther 7 (2016) 7.
[54] D.M. Shayakhmetov, Z.-Y. Li, S. Ni, A. Lieber, Analysis of adenovirus sequestration in the liver, transduction of hepatic cells, and innate toxicity after injection of fiber-modified vectors, J. Virol. 78 (2004) 5368–5381.
[55] Y. Yamamoto, M. Nagasato, T. Yoshida, K. Aoki, Recent advances in genetic modification of adenovirus vectors for cancer treatment, Cancer Sci. 108 (2017) 831–837.
[56] A.R. Yoon, D. Kasala, J. Hong, C.-O. Yun, Safety profile of EGFR-targeted hybrid vector system composed of PAMAM dendrimer and oncolytic adenovirus, J. Thorac. Dis 9 (2017) E335–E336.
[57] J.-W. Choi, S.-J. Jung, D. Kasala, J.K. Hwang, J. Hu, Y.H. Bae, C.-O. Yun, pH-sensitive oncolytic adenovirus hybrid targeting acidic tumor microenvironment and angiogenesis, J. Control. Release Off. J. Control. Release Soc 205 (2015) 134–143.
[58] A.S. Lee, C. Tang, M.S. Rao, I.L. Weissman, J.C. Wu, Tumorigenicity as a clinical hurdle for pluripotent stem cell therapies, Nat. Med. 19 (2013) 998–1004.
[59] U.S. FDA, (in) https://www.fda.gov/consumers/consumer-updates/fda-warns-about-stem-cell-therapies.